CrossMark

RESEARCH PAPER

Rheological properties of the nanofluids of tungsten oxide nanoparticles in ethylene glycol and glycerol

Mahdi Karimi-Nazarabad[1] · Elaheh K. Goharshadi[1,2] · Mohammad H. Entezari[1] · Paul Nancarrow[3,4]

Abstract In this study, nanofluids of tungsten oxide (WO_3) nanoparticles (0.5–4 % mass fractions) in ethylene glycol (EG) and glycerol (G) as base fluids were prepared and their rheological properties were measured as functions of mass fraction, temperature, and shear rate. G and WO_3–G fluids show nearly Newtonian behavior while EG and WO_3–EG fluids display shear-thinning behavior especially at higher temperatures. The experimental data were fitted to classical fluid models (power law, Bingham plastic, and Herschel–Bulkley models). The rheological behavior of both nanofluids and base fluids was fitted well with the Herschel–Bulkley model. A 9 and 14 % increase in viscosity of ethylene glycol and glycerol was observed when 4 % WO_3 nanoparticles were loaded at 20 °C and shear rates of 105 and 4 s^{-1}, respectively. The viscosity of the nanofluids decreases exponentially with increasing temperature. The viscosity data as a function of temperature were fitted with six empirical models. To the best of our knowledge, this research is the first report on the rheological properties of nanofluids of tungsten oxide nanoparticles in EG and G. The colloidal stability of both WO_3–EG and WO_3–G nanofluids was measured using UV–Vis method. It was found that the stability of WO_3–G is more than that of WO_3–EG

nanofluids. The WO_3 nanoparticles with an average particle size of 22 nm were prepared using hydrothermal method and subsequently characterized using seven techniques including X-ray diffraction, transmission electronic microscopy (TEM), high-resolution TEM, energy-dispersive X-ray spectroscopy, UV–Vis, FT-IR spectroscopy, and Doppler light scattering technique.

1 Introduction

Nanofluids are nanoscale colloidal suspensions consisting of nanometer-sized solid particles, fibers, rods, or tubes suspended in different base fluids such as water, ethylene glycol (EG), glycerol (G), and engine oil (Li et al. 2009). The study of nanofluids is an important branch of nanotechnology since they have important applications in various areas such as transportation and electronics cooling, biomedicine, and oil drilling. Nanofluids have been found to possess superior thermal conductivity compared with their base fluids (Goharshadi et al. 2013; Mahbubul et al. 2012; Nguyen et al. 2008; Rao 2010).

Most published studies have focused on the heat transfer behavior and stability of nanofluids (Abareshi et al. 2010; Abbasian Arani and Amani 2013; Ho and Chen 2013; Moosavi et al. 2010; Yeganeh et al. 2010) while very few studies have been performed on the rheological properties of nanofluids (Abareshi et al. 2011; Bobbo et al. 2012; Goharshadi and Hadadian 2012; Mariano et al. 2013; Vakili-Nezhaad and Dorany 2012). Rheological measurements are important in revealing the flow characteristics of materials and in helping formulators to select materials

✉ Elaheh K. Goharshadi
gohari@um.ac.ir

1 Department of Chemistry, Ferdowsi University of Mashhad, 91779 Mashhad, Iran

2 Center of Nano Research, Ferdowsi University of Mashhad, Mashhad, Iran

3 Department of Chemical Engineering, American University of Sharjah, Sharjah, UAE

4 School of Chemistry and Chemical Engineering, Queen's University Belfast, Belfast, UK

with optimal qualities. Parameters such as temperature, particle size and shape, particle size distribution (PSD), shear rate, surfactant, and mass fractions are known to affect the viscosity of nanofluids. Pastoriza-Gallego et al. (2011) investigated the viscosity of nanofluids consisting of CuO nanoparticles (NPs) in water for different particle sizes and mass fractions. Samples containing smaller NPs were found to exhibit higher viscosity for the same mass loading. Servais et al. (2002) and Genovese (2012) showed the effect of increasing the PSD for a given particle mass fraction is to increase the effective maximum packing fraction and thus decrease the viscosity. Namburu et al. (2007a) showed that the viscosity of the nanofluids containing SiO_2 NPs in EG and water as base fluids decreases exponentially with increasing temperature for a temperature range of 35–50 °C. They also found that the nanofluids demonstrate non-Newtonian behavior at low temperatures and behave as Newtonian fluids at high temperatures. Abareshi et al. (2011) investigated the effect of temperature and mass fraction on the viscosity of colloidal α-Fe_2O_3 NPs in G and found that although G shows Newtonian behavior, the nanofluids are non-Newtonian fluids with shear-thinning behavior. Nguyen et al. (2008) found that the nanofluid viscosity increases considerably with NPs mass fraction but decreases with increasing temperature.

Oxide nanomaterials are the key ingredients for the development of many advanced functional materials and smart devices. In particular, WO_3 NPs have unique optical, electrical, and structural properties and wide variety of applications in chemical and selective catalysis, mechanical sensors, electrochemical industry, antimicrobial, and environment (Cui et al. 2008; Deb 2008; Georgieva et al. 2011; Gondal et al. 2009, 2010; Patzke et al. 2011; Svensson and Granqvist 1984; Wang et al. 2008; Zheng et al. 2011). Much of these applications require the dispersion of WO_3 NPs in a base fluid to form a nanofluid.

Ethylene glycol is used in a variety of consumer and industrial applications. The compound is frequently used as basic building block for some chemicals, anti-freeze fluids, polyester fiber, polyester resins, the manufacture of asphalt emulsion paints, heat transfer agents, brake fluids, in miscellaneous industrial applications such as solvents, floor and wall adhesives, automotive wax/polish, and floor wax/polish (Staples et al. 2001; Taherzadeh et al. 2002). Glycerol is used in foods and cosmetics, tobacco, wrapping and packaging materials, lubricants, urethane polymers, gaskets, cork products, cement compounds, soldering compounds, compasses, cleaning materials, detergents, wetting agents, emulsifiers, skin protectives, asphalt, ceramics, photographic products, leather and wood treatment, and adhesives (Taherzadeh et al. 2002).

The main goal of the present work is to prepare the nanofluids of WO_3 NPs in EG and G and measure their rheological properties as functions of temperature, mass fraction, and shear rate. For this purpose, WO_3 NPs were prepared using sodium tungstate as a precursor by a facile hydrothermal method. Then, WO_3 nanofluids were prepared and characterized by a variety of methods. Also, the stability of WO_3 nanofluids was estimated using UV–Vis method.

2 Experimental

2.1 Synthesis procedure

The amount of 30 ml hydrochloric acid aqueous solution (4 M) was added dropwise to 20 ml aqueous solution of sodium tungstate, $Na_2WO_4 \cdot 2H_2O$ (0.05 M), and stirred for 1 h at room temperature. The solution was then introduced into a Teflon tube and autoclaved at 60 °C for 24 h. The yellow precipitate was separated by centrifuging, washed several times with double distilled water, and air-dried in a furnace at 250 °C for 3 h. All chemicals were of analytical grade and used as received without further purification.

2.2 Characterization techniques

The XRD measurements were carried out with a Bruker/D8 ADVANCED diffractometer using Cu Kα radiation ($\lambda = 0.15406$ nm) in the range of $2\theta = 10º–70º$ by the step of 0.05. The size and shape of the WO_3 NPs were examined by a LEO 912 AB transmission electron microscope. The electron beam accelerating voltage was 120 kV.

The Fourier transform infrared (FT-IR) spectrum was recorded at room temperature with a KBr pellet on a Shimadzu 4300 spectrometer ranging from 500 to 4000 cm^{-1}.

The high-resolution TEM (HRTEM) was used to investigate the crystalline nature of NPs by FEITecnai F20 Field emission with the acceleration voltage of 200 kV. The energy-dispersive X-ray (EDX) analyses were provided using the LEO 1450 VP Model.

The UV–Vis absorbance spectra were obtained using an Agilent photodiode-array Model 8453 equipped with quartz cell of 1 cm path length. The spectra were recorded at room temperature in air within the range 200–1100 nm. The DLS measurements were obtained using a particle size analyzer CORDOUAN model VASCO3.

2.3 Preparation of nanofluids

WO_3 NPs were dispersed in EG and G with the help of an ultrasonic processor (Sonicator 4000) with a frequency of 20 kHz for 20 min. The power transferred to the solution was 33 W cm^{-2} as measured by the calorimetric method.
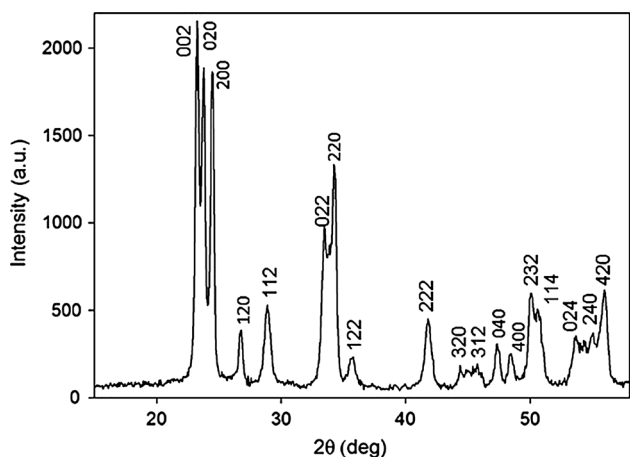
Fig. 1 X-ray diffraction pattern of the WO$_3$ NPs

Fig. 2 FT-IR spectrum of WO$_3$ NPs

The viscosity were measured using a Brookfield Viscometer (LV DV-II + Pro EXTRA, spindle: SC4-18) with a small sample adaptor. The temperature was controlled by circulating water through the cylindrical jacket (BL 7100, Major Science). The measurements were performed on nanofluids of different WO$_3$ mass fraction between 0 and 4 and the temperatures between 20 and 60 °C.

3 Results and discussion

3.1 Characterization

Figure 1 shows the XRD pattern of WO$_3$ NPs. The diffraction peaks can be assigned to both monoclinic (ICDD No. 00-043-1035) and orthorhombic (ICDD No. 00-020-1324) phases since the peaks overlap with each other (Zheng et al. 2010). The strong intensity and narrow width of WO$_3$ diffraction peaks indicate that the resulting products are of high crystallinity. The XRD pattern shows no extra diffraction peaks, indicating that the WO$_3$ NPs were prepared to a high level of purity.

The average crystallite size was estimated using the Scherrer formula:

$$D_{hkl} = \frac{k \times \lambda}{\beta_{hkl} \times \cos\theta_{hkl}} \quad (1)$$

where D_{hkl} is the crystallite size of (hkl) plane, k is a constant (0.9), β_{hkl} is the full width at half maximum of the (hkl) diffraction peak, θ_{hkl} is the Bragg angle of (hkl) peak, and λ is the wavelength of X-ray ($\lambda = 0.154056$ nm for Cu Kα radiation). The average crystallite size of WO$_3$ NPs according to the Debye–Scherrer equation was around 19 nm.

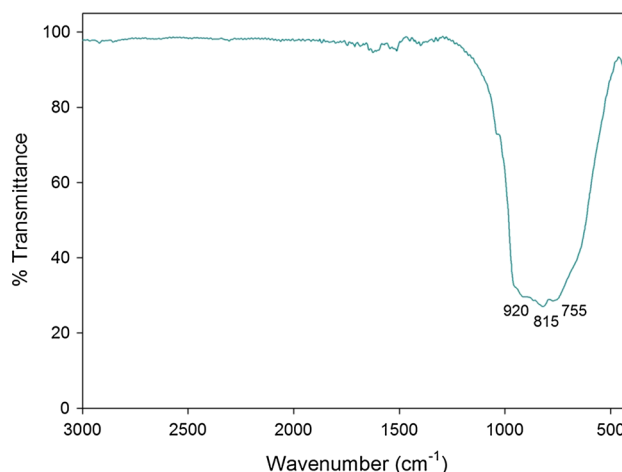Figure 2 shows the FT-IR spectrum of WO$_3$ NPs. The FT-IR spectrum of WO$_3$ NPs shows three strong absorption bands at 755, 815, and 920 cm^{-1} which overlap. The peaks can be assigned to O–W–O stretching vibrations (Daniel et al. 1987; Goodenough et al. 1984).

The TEM image and the PSD histogram of WO$_3$ NPs are shown in Fig. 3a. The average particle size obtained was around 22 nm which is in reasonably close agreement with the XRD result. The HRTEM images of WO$_3$ NPs (Fig. 3) show the presence of regular sets of lattice fringes corresponding to interplanar spacings that are characteristic of WO$_3$ crystallites. The interplanar distance values of 0.322 and 0.306 nm can be assigned to the (120) and (112) crystal planes of monoclinic or orthorhombic WO$_3$, respectively.

The energy-dispersive X-ray (EDX) analysis showed four high-intensity peaks at 1.4, 1.8, 8.4, and 9.6 keV corresponding to the presence of W, a single peak for O at 0.5 keV. The W/O atomic ratio of 1:3 is consistent with a pure WO$_3$ phase.

Figure 4a shows the measured UV–visible spectrum of the WO$_3$ NPs; a main absorbance peak at about 380 nm (Smith et al. 2007) is observed. The absorbance peak of WO$_3$ NPs was shifted to smaller wavelength compared with WO$_3$ bulk (480 nm) (Goodenough et al. 1984). It is widely accepted that this observed blueshift can be attributed to the quantum confinement effect. This causes indirect perturbation of the electronic wave function due to Coulomb effects and results in more subtle changes in the band gap energy (Yoffe 1993).

The band gap, E_g, of WO$_3$ NPs (it is an indirect semiconductor) was calculated using Tauc equation (Tauc et al. 1966):

$$(\alpha h\nu)^{1/2} = K(h\nu - E_g) \quad (2)$$

where α is the absorption coefficient, $h\nu$ is the incident photon energy, and K is a constant. The band gap value of WO$_3$ was found to be 3.03 eV (inset of Fig. 4a). The same

Fig. 3 a PSD calculated using TEM image (*inset*), **b**, **c** HRTEM images of WO$_3$ NPs
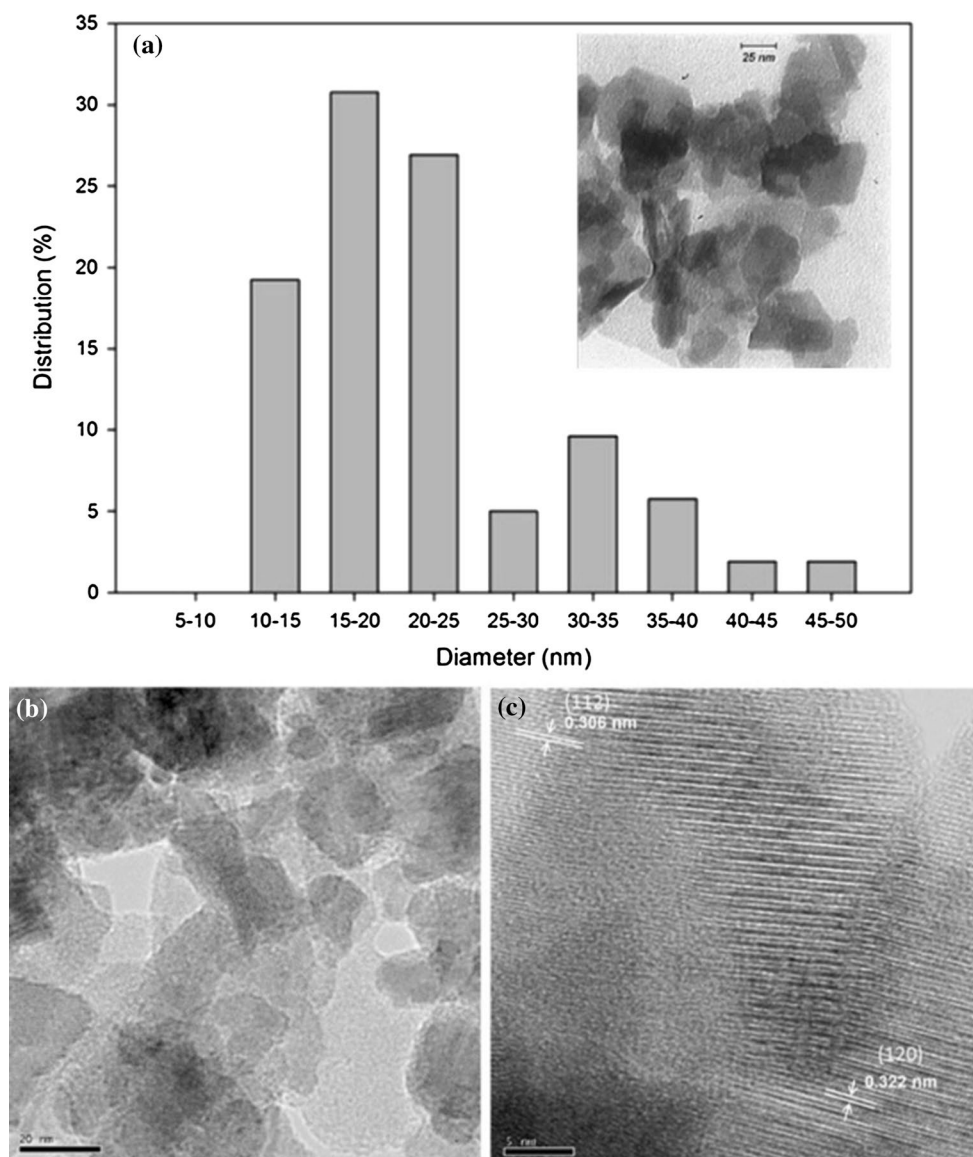
value was obtained by plotting the derivation of logarithm of Eq. 2 versus *hν;*

$$\frac{d[\ln(\alpha h\nu)]}{d(h\nu)} = \frac{2}{h\nu - E_g} \qquad (3)$$

and set equal to zero (Fig. 4b). Due to the quantum size effect, the energy band gap of the WO$_3$ NPs is larger than that of the WO$_3$ bulk (2.6 eV) (Goodenough et al. 1984).

The PSD of both nanofluids was measured by DLS technique (Fig. 5). The average particle size is about 50 and 2 nm in WO$_3$–EG and WO$_3$–G nanofluids, respectively.

3.2 The rheological data

A flow curve (the curve of viscosity, η, vs. shear rate, $\gamma°$) can provide important information about storage stability, optimal pumping, and transferring. The viscosity values of both base fluids, namely EG and G, were measured as a function of shear rate between 20 and 60 °C as shown in Fig. 6. The viscosity values of both fluids decrease with the shear rate at lower shear rates and at lower temperatures, indicating non-Newtonian behavior but act as Newtonian fluid at higher shear rates. The viscosity of G is greater than that of EG at constant temperature and shear rate because the hydrogen bonds in G are stronger than those of EG. The viscosity values of both EG and G decrease as the temperature increases because the hydrogen bonds between the molecules become weaker.

3.2.1 Influence of shear rate

Figure 7a and b shows viscosity versus shear rate for the nanofluids containing 4 % WO$_3$ NPs in EG and G,
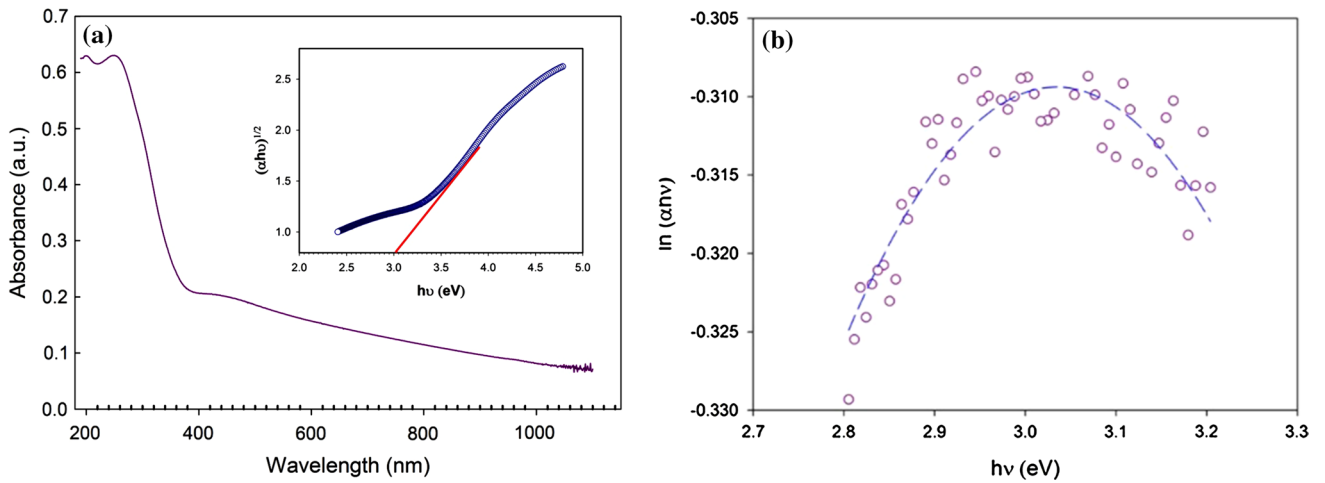
Fig. 4 **a** UV–Vis spectrum of WO$_3$ NPs dispersed in water. Plot of $(\alpha h\nu)^{1/2}$ versus photon energy (*inset*), **b** the plot of $\ln(\alpha h\nu)$ versus photon energy. The *circles* are experimental values and the *dashed line* is curve fitting
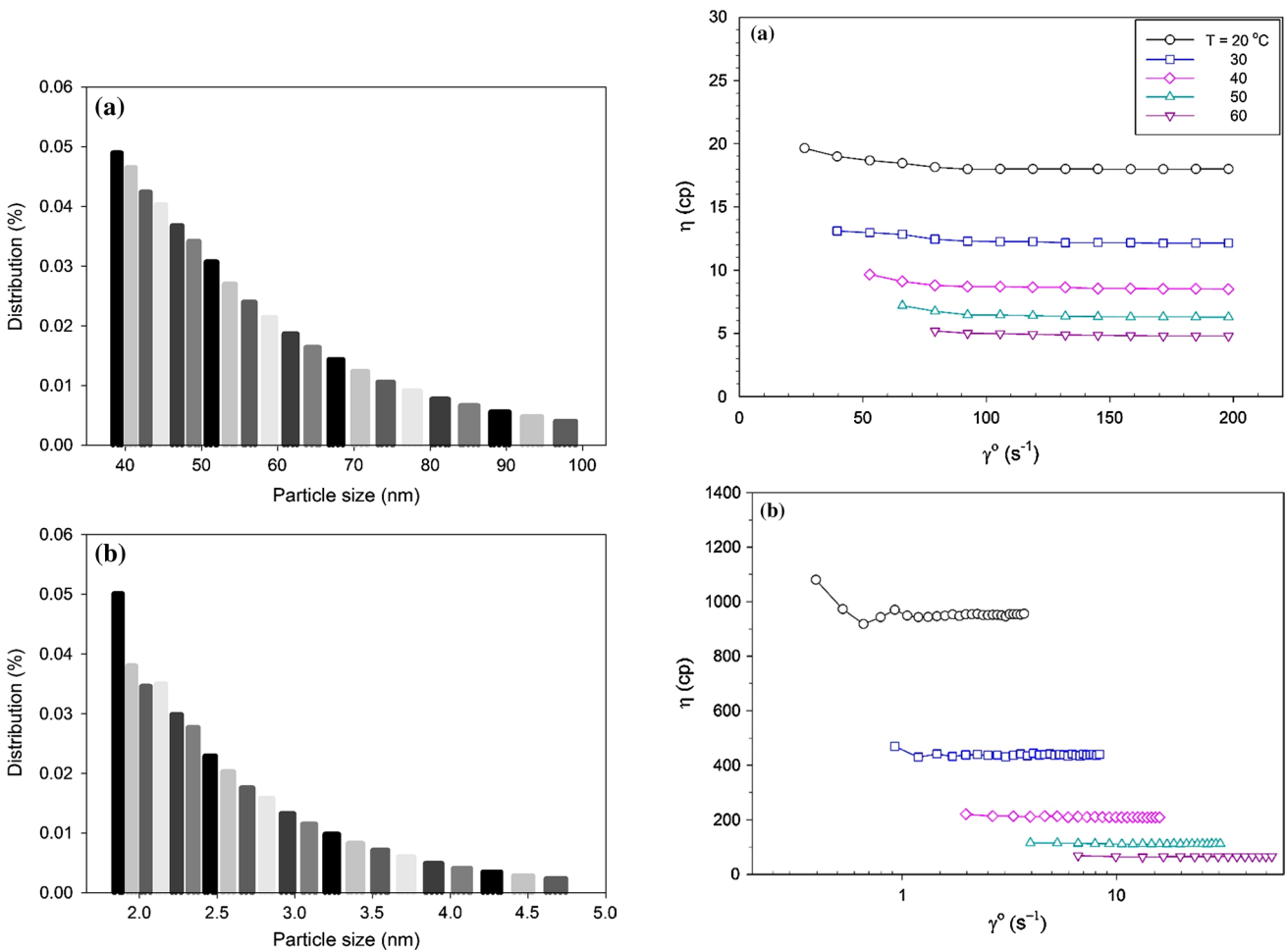

Fig. 5 PSD of 0.01 % **a** WO$_3$–EG and **b** WO$_3$–G nanofluid

Fig. 6 Viscosity versus shear rate at different temperatures for **a** EG and **b** G
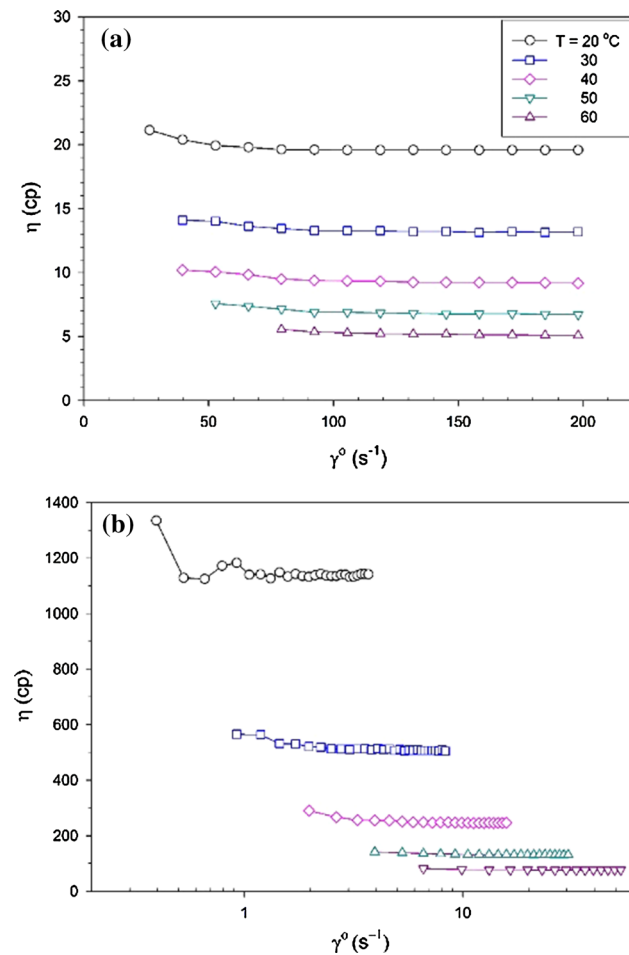
Fig. 7 Viscosity versus shear rate of the nanofluids containing 4 % WO$_3$ NPs at different temperatures in **a** EG and **b** G

respectively at different temperatures. The existence of Newtonian or non-Newtonian behaviors in nanofluids depends strongly on many factors such as the type, size, shape, mass fraction of NPs, and temperature. At lower shear rates, the viscosity of nanofluids decreases with increasing shear rate, indicating shear-thinning behavior. As shear rate increases, the individual particles which make up the aggregate give up their intermolecular forces, start to break apart, and align in the direction of increased shear rate. This loss or decline in resistance to flow results in a decreased viscosity of the fluid (Aladag et al. 2012). At high shear rates, the viscosity of nanofluids attains a limiting and constant value, suggesting that the interactions become relatively weak. Also, nanofluids are well known as structured materials with particles or aggregates even at low mass fraction. By increasing shear rate, the structure and the flocculants of the nanofluid break down and hence viscosity decreases. Inversely, reducing the shear rate can cause a growth of

the flocculants and/or allow the particulate network to rebuild (Aladag et al. 2012). The strong non-Newtonian behavior of WO$_3$ nanofluids at low shear rates is similar to those of observed by Aladag et al. (2012) for Al$_2$O$_3$–water nanofluids, He et al. (2007) for TiO$_2$–water nanofluids, and Abareshi et al. (2011) for α-Fe$_2$O$_3$–G nanofluids. As Fig. 7 shows, the influence of temperature on the viscosity of the WO$_3$–G nanofluid is greater than that for the WO$_3$–EG nanofluid.

In order to the study the flow behavior of both base fluids and nanofluids, the experimental data were fitted to the classical fluid rheological models (power law model, Bingham plastic model, and Herschel–Bulkley model) at different temperatures (20, 30, 40, 50, and 60 °C). The rheological models considered are given below:

3.2.1.1 Power law model

$$\tau = K\gamma^n \tag{4}$$

where K is the consistency index (Pa s^n), n is the flow behavior index (dimensionless), and γ is the shear rate (s^{-1}). Three cases may occur: n may be equal to, less than, or greater than one. In these cases, the nanofluid is Newtonian, pseudoplastic (the plot of shear stress against shear strain passes through the origin), or Bingham (fluids that have a linear shear stress/shear rate relationship and require a finite yield stress before they begin to flow), or dilatant, respectively.

3.2.1.2 Bingham plastic model

$$\tau = \tau_o + \mu_p\gamma \tag{5}$$

where τ_o is the yield stress and μ_p is the plastic viscosity (cP).

3.2.1.3 Herschel–Bulkley model

$$\tau = \tau_o + K\gamma^n \tag{6}$$

Tables 1 and 2 give the fit values of constants of the models (Eqs. 4–6) considered in this study. As these tables show that the Herschel–Bulkley model fits better with the experimental data compared with other models. The fluids of this work show non-Newtonian behavior and hence their viscosity dependent on shear rate, and exhibit shear-thinning behavior at low shear rates, i.e., their viscosity decreases with increasing shear rate. The power law model underestimates the low shear rate viscosity of fluids since it considers zero value for the shear stress at zero shear rate. The Bingham model considers the fluids to have a yield value. The Herschel–Bulkley model is a hybrid of power law and Bingham models.

Lower values of n are an indication of a more non-Newtonian behavior or a shear-thinning fluid. In general

Table 1 Constants for rheological models for EG and WO$_3$–EG

f_m	T (°C)	Power law			Bingham plastic			Herschel–Bulky			
		K	n	R^2	τ_o	μ_p	R^2	τ_o	K	n	R^2
0	20	0.20	0.98	0.9997	0.42	0.18	0.9997	0.78	0.16	1.023	0.9998
	30	0.15	0.96	0.9996	0.54	0.12	0.9999	0.80	0.10	1.025	0.9999
	40	0.12	0.94	0.9994	0.55	0.08	0.9997	0.63	0.08	1.012	0.9997
	50	0.10	0.91	0.9985	0.59	0.06	0.9991	0.66	0.05	1.014	0.9992
	60	0.09	0.88	0.9957	0.60	0.04	0.9961	0.44	0.05	0.962	0.9962
0.5	20	0.21	0.98	0.9996	0.55	0.18	0.9998	1.33	0.14	1.050	0.9999
	30	0.16	0.96	0.9995	0.54	0.13	0.9998	0.96	0.10	1.039	0.9999
	40	0.13	0.93	0.9989	0.62	0.09	0.9995	0.94	0.07	1.043	0.9996
	50	0.11	0.90	0.9979	0.68	0.06	0.9990	0.89	0.05	1.040	0.9991
	60	0.10	0.88	0.9965	0.65	0.05	0.9977	0.70	0.04	1.013	0.9977
1	20	0.21	0.98	0.9998	0.39	0.19	0.9999	0.89	0.16	1.031	0.9999
	30	0.16	0.96	0.9997	0.51	0.13	0.9999	0.84	0.11	1.030	0.9999
	40	0.12	0.95	0.9995	0.47	0.09	0.9998	0.74	0.07	1.035	0.9999
	50	0.10	0.93	0.9991	0.52	0.06	0.9997	0.64	0.06	1.022	0.9997
	60	0.08	0.90	0.9989	0.50	0.05	0.9995	0.50	0.05	1.001	0.9995
2	20	0.21	0.99	0.9999	0.30	0.19	0.9999	0.54	0.17	1.015	0.9999
	30	0.15	0.97	0.9998	0.41	0.13	0.9999	0.66	0.11	1.023	0.9999
	40	0.11	0.96	0.9998	0.38	0.09	0.9999	0.32	0.09	0.992	0.9999
	50	0.09	0.94	0.9998	0.37	0.06	0.9997	0.07	0.08	0.950	0.9998
	60	0.07	0.93	0.9993	0.35	0.05	0.9995	0.27	0.05	0.981	0.9995
4	20	0.21	0.99	0.9998	0.28	0.20	0.9999	0.91	0.16	1.038	0.9999
	30	0.16	0.97	0.9997	0.47	0.13	0.9999	0.76	0.11	1.026	0.9999
	40	0.12	0.94	0.9995	0.54	0.09	0.9999	0.75	0.08	1.027	0.9999
	50	0.10	0.93	0.9994	0.47	0.06	0.9996	0.42	0.07	0.992	0.9996
	60	0.10	0.90	0.9993	0.52	0.05	0.9995	0.36	0.06	0.964	0.9996

as Table 1 shows, by increasing temperature the value of n decreases for EG and WO$_3$–EG, i.e., by raising temperature, the shear-thinning behavior of the fluids increases. As Table 1 shows, EG and WO$_3$–EG fluids exhibit non-Newtonian behavior with shear-thinning behavior for all mass fractions, especially at 60 °C, while G and WO$_3$–G fluids display somewhat nearly Newtonian behavior. The non-Newtonian behavior was also observed by Abareshi et al. (2011) for α-Fe$_2$O$_3$–G nanofluid, Moosavi et al. (2010) for ZnO–G and ZnO–EG nanofluids, and Aladag et al. (2012) for Al$_2$O$_3$–water nanofluids.

3.2.2 Influence of nanoparticles mass fraction

Figure 8 shows the values of nanofluid viscosity as a function of shear rate for different mass fractions. The non-Newtonian character of the fluids is more obvious at higher NP mass fractions and lower shear rates. The viscosity of the WO$_3$–EG nanofluid increases when mass fraction increases (Fig. 8a) in agreement with previous studies (Abareshi et al. 2011; Moosavi et al. 2010; Nguyen et al. 2008). By increasing the concentration of solid particles in a suspension, the nanofluid becomes progressively chaotic and aggregate form and hence the viscosity increases. Figure 8b shows the flow curve at 20 °C for the WO$_3$–G nanofluids at shear rate of 4 s^{-1}. The viscosity of nanofluids containing 1 and 2 % WO$_3$ due to lubricating effect of NPs (Chen et al. 2008) is lower than that of 0.5 % WO$_3$. It means the WO$_3$–G nanofluids show different behavior with respect to WO$_3$–EG nanofluid. Certainly, the interactions of WO$_3$ NPs with G molecules differ with EG molecules. The increase in viscosity, $\frac{\eta_{nf}-\eta_{bf}}{\eta_{bf}} \times 100$ (η_{bf} and η_{nf} are the viscosity of base fluid and nanofluid at the same temperature and shear rate), of the WO$_3$–EG and WO$_3$–G nanofluids at different temperatures and mass fractions under constant shear rate is summarized in Table 3. A maximum of 8.7 % (14.3 %) increase in the viscosity of EG (G) at 20 °C is observed when the mass fraction of WO$_3$ NPs was 0.04. As this table shows, the increase in viscosity for WO$_3$–G is more than that for WO$_3$–EG due to stronger interactions between WO$_3$ and G.

Table 2 Constants of rheological models for G and WO$_3$–G

f_m	T (°C)	Power law			Bingham plastic			Herschel–Bulky			
		K	n	R^2	τ_o	μ_p	R^2	τ_o	K	n	R^2
0	20	9.61	0.99	0.9995	0.17	9.49	0.9996	0.79	8.86	1.042	0.9997
	30	4.39	1.00	0.9998	0.01	4.39	0.9998	0.05	4.36	1.003	0.9998
	40	2.21	0.98	0.9998	0.32	2.08	0.9998	0.20	2.13	0.992	0.9998
	50	1.14	0.99	0.9997	0.18	1.11	0.9998	0.83	0.94	1.044	0.9999
	60	0.66	1.00	0.9997	0.09	0.65	0.9997	0.65	0.55	1.038	0.9998
0.5	20	10.65	0.99	0.9998	0.24	10.44	0.9999	0.48	10.19	1.015	0.9999
	30	4.70	0.98	0.9999	0.29	4.52	1.000	0.45	4.41	1.010	1.000
	40	2.35	0.98	0.9995	0.48	2.18	0.9997	1.28	1.84	1.055	0.9999
	50	1.24	0.98	0.9999	0.30	1.17	0.9999	0.66	1.07	1.023	0.9999
	60	0.70	0.99	0.9999	0.17	0.67	0.9999	0.31	0.65	1.009	0.9999
1	20	10.87	0.98	0.9996	0.51	10.41	0.9997	0.90	10.01	1.024	0.9997
	30	4.92	0.97	0.9998	0.50	4.62	0.9999	0.67	4.50	1.010	0.9999
	40	2.41	0.98	0.9997	0.43	2.25	0.9998	0.85	2.07	1.026	0.9999
	50	1.03	0.98	0.9996	0.49	1.16	0.9998	1.22	1.00	1.046	0.9999
	60	0.72	0.99	0.9998	0.19	0.70	0.9999	0.80	0.59	1.038	1.000
2	20	10.68	0.99	0.9992	0.35	10.40	0.9993	1.08	9.66	1.046	0.9994
	30	4.87	0.97	0.9990	0.69	4.48	0.9993	1.48	3.96	1.050	0.9994
	40	2.39	0.97	0.9992	0.59	2.18	0.9995	1.51	1.79	1.063	0.9998
	50	1.26	0.98	0.9997	0.37	1.18	0.9998	0.67	1.10	1.019	0.9998
	60	0.74	0.98	0.9998	0.35	0.69	0.9999	0.75	0.62	1.025	0.9999
4	20	11.40	1.00	0.9996	0.12	11.35	0.9996	0.90	10.56	1.045	0.9997
	30	5.34	0.97	0.9997	0.58	5.00	0.9998	1.10	4.66	1.029	0.9999
	40	2.67	0.97	0.9993	0.70	2.42	0.9996	1.69	2.00	1.061	0.9998
	50	1.40	0.98	0.9998	0.45	1.30	0.9999	1.02	1.15	1.033	0.9999
	60	0.80	0.99	0.9998	0.32	0.76	0.9999	0.88	0.66	1.033	0.9999

3.2.3 Influence of temperature

As temperature increases, the viscosity of both base fluids and the nanofluids decreases exponentially (Fig. 9) in agreement with previous studies (Abareshi et al. 2011; Haisheng et al. 2007; Namburu et al. 2007b). The decrease in viscosity with raising temperature is somewhat compromised by increasing the mass fraction of WO$_3$. The results show that with 10 °C increase in temperature, the values of viscosity of the nanofluids decrease approximately 0.7 and 0.5 times for EG and G, respectively. The difference between viscosity of the nanofluids reduces at high temperatures because the interactions between the NPs and base fluid molecules become weaker. When the temperature increases, the interaction time between neighboring molecules of a fluid decreases due to increased velocities of individual molecules. High temperature also influences the Brownian motion of NPs and hence decreases the viscosity of nanofluids. As Fig. 9 shows, the influence of temperature

on viscosity for WO$_3$–G nanofluids is greater than that for WO$_3$–EG nanofluids.

The temperature dependence of the viscosity of nanofluids is described reasonably by different empirical correlations (Table 4). The experimental data were fitted with six empirical models, namely Vogel–Fulcher–Tammann (Chen et al. 2007), White (2005), Reid et al. (1977), Yaws (1997), Kulkarni et al. (2006), and Namburu et al. (2007b) equations. The data presented here were found to fit well with the Namburu equation:

$$\log(\eta_{nf}) = A \exp(BT) \tag{7}$$

where A and B are functions of particle mass fraction (Table 5) and fitted with the following equations:

$$A = a_1 + a_2 f_m + a_3 f_m^2 \tag{8}$$

$$B = b_1 + b_2 f_m + b_3 f_m^2 \tag{9}$$
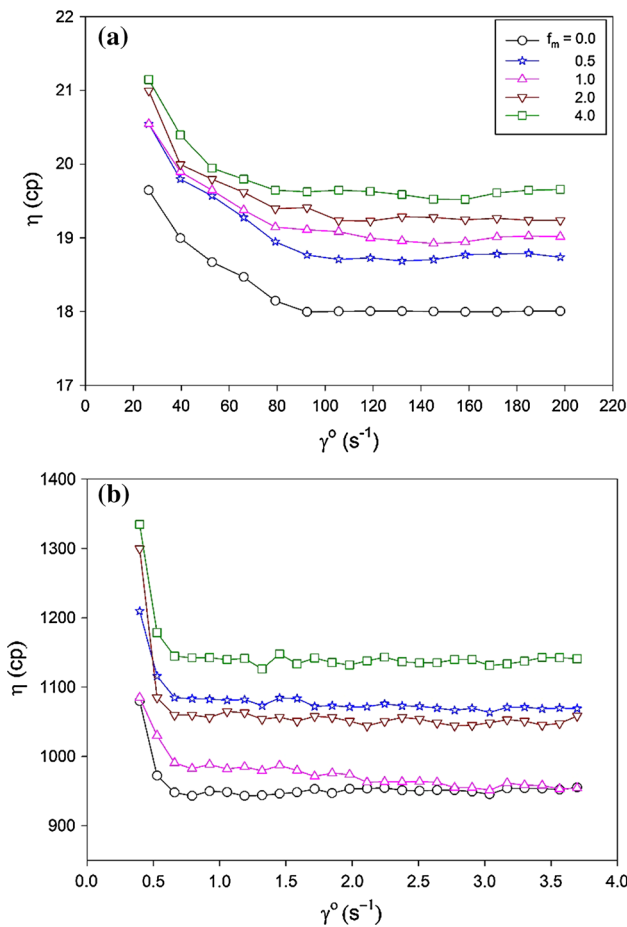
The constants of Eqs. 8 and 9 are given in Table 6.

Fig. 8 Viscosity versus shear rate at 20 °C at different mass fractions for the nanofluids of **a** WO$_3$–EG at shear rate of 105 s^{-1}, **b** WO$_3$–G at shear rate of 4 s^{-1}

Table 3 Increase in viscosity of the WO$_3$–EG and WO$_3$–G nanofluids for the shear rates 105 and 4 s^{-1}, respectively

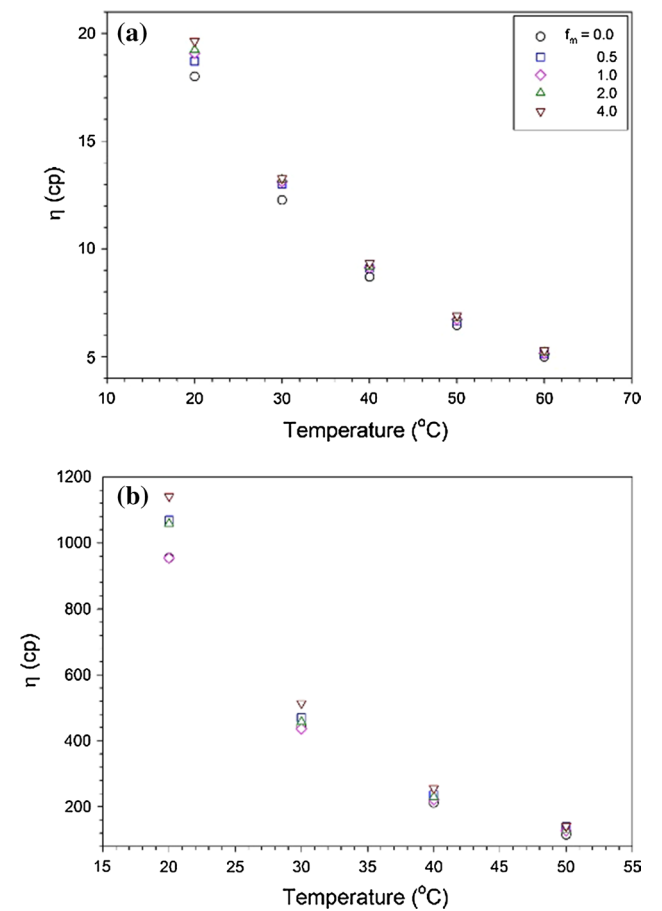| T (°C)	f_m	Enhancement in viscosity	
		WO$_3$–EG	WO$_3$–G
20	0.005	3.9	10.7
	0.010	6.0	9.4
	0.020	6.8	11.4
	0.040	8.7	14.3
30	0.005	6.1	8.4
	0.010	7.0	9.2
	0.020	6.1	9.8
	0.040	8.2	12.4
40	0.005	5.6	4.6
	0.010	6.0	5.1
	0.020	5.6	8.0
	0.040	7.4	8.4
50	0.005	5.7	3.8
	0.010	5.7	7.6
	0.020	3.8	8.4
	0.040	7.0	10.7

Fig. 9 Viscosity versus temperature at different mass fraction for the nanofluids of **a** WO$_3$–EG at shear rate of 105 s^{-1}, **b** WO$_3$–G at shear rate of 4 s^{-1}

3.3 Colloidal stability

The colloidal stability of nanofluids is a challenging subject. Nanoparticles tend to aggregate with the time elapsed for its high surface activity. The UV–Vis measurements have been used to quantitatively characterize colloidal stability of the dispersions (Jiang et al. 2003). Figure 10 shows the UV–Vis absorption spectra of both nanofluids versus sedimentation time for WO$_3$ mass fraction of 0.01 %. As this figure shows, the absorption of WO$_3$–EG nanofluid with sediment time changes to some extent but the changes for WO$_3$–G nanofluid are very little. Hence, the WO$_3$–G nanofluid is much more stable than WO$_3$–G nanofluid. The maximum absorption wavelength of the WO$_3$–EG and WO$_3$–G nanofluids is around 269 and 265 nm, respectively. Since there was a linear relation between the WO$_3$ mass fraction and the absorbance of the nanofluids, the relative stability was estimated with sediment time as 14 and 75 % for the

Table 4 Temperature dependence of the nanofluid viscosity equations

Equation[a]	Constant parameters	References
$\eta(T) = \exp\left(\frac{B}{T+T_0}\right)$	B, T_0	Chen et al. (2007), Haisheng et al. (2007)
$\ln \frac{\eta_{nf}}{\eta_{bf}} = a + b\left(\frac{T_0}{T}\right) + c\left(\frac{T_0}{T}\right)^2$	a, b, T_0	White (2005)
$\eta_{nf} = A \exp\left(B/T\right)$	A, B	Reid et al. (1977)
$\log(\eta_{nf}) = A + BT^{-1} + CT + DT^2$	A, B, C, D	Yaws (1997)
$\ln(\eta_{nf}) = AT^{-1} - B$	A, B	Kulkarni et al. (2006)
$\log(\eta_{nf}) = A \exp(BT)$	A, B	Namburu et al. (2007b)

[a] η_{bf} and η_{nf} represent the viscosity of base fluid and nanofluid, respectively

Table 5 Namburu parameters (Eq. 7) for WO_3–EG and WO_3–G at the constant shear rates 105 and 4 s^{-1}, respectively

f_m	WO_3–EG			WO_3–G		
	A	B	R_{sqr}	A	B	R_{sqr}
0.000	1.686	−0.0147	0.9999	3.834	−0.0119	0.9997
0.005	1.701	−0.0143	0.9996	3.909	−0.0121	0.9994
0.010	1.713	−0.0144	0.9997	3.910	−0.0120	0.9993
0.020	1.726	−0.0146	0.9999	3.911	−0.0120	0.9993
0.040	1.730	−0.0145	0.9999	3.921	−0.0120	0.9994

Table 6 Constants of Eqs. 8 and 9

Nanofluid	a_1	$a_2 \times 10^{-3}$	$a_3 \times 10^{-3}$	R_{sqr}	$b_1 \times 10^{-2}$	$b_2 \times 10^{-5}$	$b_3 \times 10^{-5}$	R_{sqr}
WO_3–EG	1.69	29.9	−4.80	1.00	−1.41	−40.00	6.99	0.98
WO_3–G	3.91	−1.0	1.00	1.00	−1.19	−8.59	1.59	0.98

WO_3–EG and WO_3–G nanofluids, respectively within 15 days.

4 Conclusions

Tungsten oxide NPs were successfully prepared by the hydrothermal method. The NPs were characterized by seven techniques which confirmed the presence of pure nanocrystals. The rheological properties of nanofluid prepared from WO_3 NPs suspended in EG and G were measured as functions of temperature and mass fraction. This study contains the following main points:

- Both base fluids and nanofluids behave as shear-thinning fluids especially at lower shear rates. G and WO_3–G fluids show somewhat nearly Newtonian behavior while EG and WO_3–EG fluids display shear-thinning behavior especially at higher temperatures.

- The viscosity of the nanofluids is strongly influenced by the NPs mass fraction. The viscosity of the WO_3–EG nanofluids increases with increasing mass fraction of NPs. The viscosity of WO_3-G does not follow a specific behavior with mass fraction.

- The rheological properties of both base fluids and the nanofluids decrease exponentially with increasing temperature. The experimental data of nanofluids viscosity as a function of temperature were fitted by six empirical models. The Namburu equation gave a reasonable prediction of rheological properties of WO_3–EG and WO_3–G nanofluids.

- A 9 and 14 % increase in viscosity of EG and G was observed at 20 °C by loading of 4 % WO_3 NPs at shear rate 105 and 4 s^{-1}, respectively.

- The stability of both nanofluids was measured by UV–Vis method. The UV–Vis analysis reveals that stability of WO_3–G nanofluid is much more than that of WO_3–EG nanofluid.
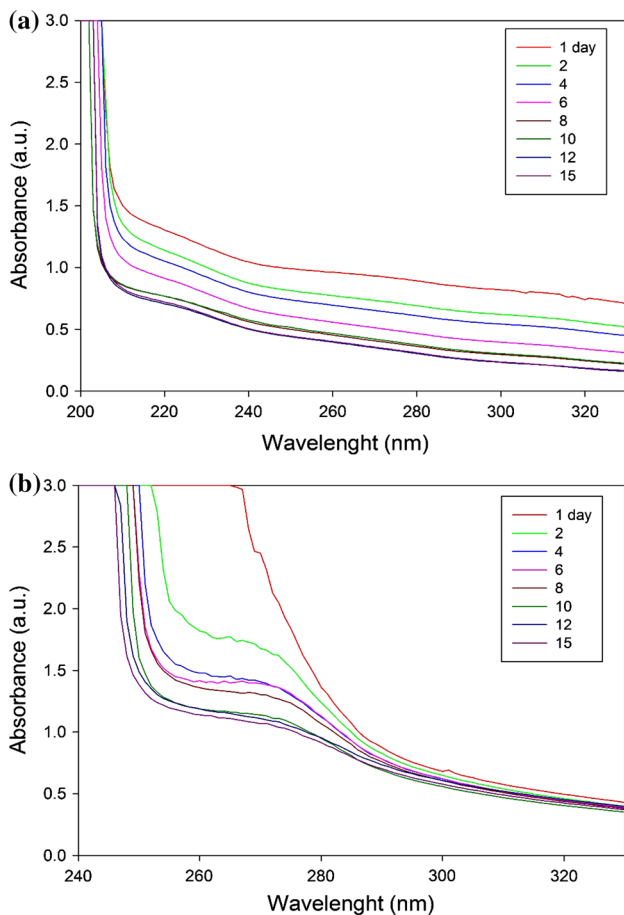
Fig. 10 UV–Vis spectrum of 0.01 % **a** WO_3–EG and **b** WO_3–G nanofluid

References

Abareshi M, Goharshadi EK, Mojtaba Zebarjad S, Khandan Fadafan H, Youssefi A (2010) Fabrication, characterization and measurement of thermal conductivity of Fe_3O_4 nanofluids. J Magn Magn Mater 322:3895–3901. doi:10.1016/j.jmmm.2010.08.016

Abareshi M, Sajjadi SH, Zebarjad SM, Goharshadi EK (2011) Fabrication, characterization, and measurement of viscosity of α-Fe_2O_3–glycerol nanofluids. J Mol Liq 163:27–32. doi:10.1016/j.molliq.2011.07.007

Abbasian Arani AA, Amani J (2013) Experimental investigation of diameter effect on heat transfer performance and pressure drop of TiO_2–water nanofluid. Exp Therm Fluid Sci 44:520–533. doi:10.1016/j.expthermflusci.2012.08.014

Aladag B, Halelfadl S, Doner N, Maré T, Duret S, Estellé P (2012) Experimental investigations of the viscosity of nanofluids at low temperatures. Appl Energy 97:876–880. doi:10.1016/j.apenergy.2011.12.101

Bobbo S, Fedele L, Benetti A, Colla L, Fabrizio M, Pagura C, Barison S (2012) Viscosity of water based SWCNH and TiO_2 nanofluids. Exp Therm Fluid Sci 36:65–71. doi:10.1016/j.expthermflusci.2011.08.004

Chen H, Ding Y, He Y, Tan C (2007) Rheological behaviour of ethylene glycol based titania nanofluids. Chem Phys Lett 444:333–337. doi:10.1016/j.cplett.2007.07.046

Chen L, Xie H, Li Y, Yu W (2008) Nanofluids containing carbon nanotubes treated by mechanochemical reaction. Thermochim Acta 477:21–24. doi:10.1016/j.tca.2008.08.001

Cui X, Shi J, Chen H, Zhang L, Guo L, Gao J, Li J (2008) Platinum/mesoporous WO_3 as a carbon-free electrocatalyst with enhanced electrochemical activity for methanol oxidation. J Phys Chem B 112:12024–12031. doi:10.1021/jp803565k

Daniel MF, Desbat B, Lassegues JC, Gerand B, Figlarz M (1987) Infrared and raman study of WO_3 tungsten trioxides and WO_3, xH_2O tungsten trioxide tydrates. J Solid State Chem 67:235–247. doi:10.1016/0022-4596(87)90359-8

Deb SK (2008) Opportunities and challenges in science and technology of WO_3 for electrochromic and related applications. Sol Energy Mater Sol Cells 92:245–258. doi:10.1016/j.solmat.2007.01.026

Genovese DB (2012) Shear rheology of hard-sphere, dispersed, and aggregated suspensions, and filler-matrix composites. Adv Colloid Interface Sci 171–172:1–16. doi:10.1016/j.cis.2011.12.005

Georgieva J, Sotiropoulos S, Armyanov S, Philippidis N, Poulios I (2011) Photoelectrocatalytic activity of bi-layer TiO_2/WO_3 coatings for the degradation of 4-chlorophenol: effect of morphology and catalyst loading. J Appl Electrochem 41:173–181. doi:10.1007/s10800-010-0221-8

Goharshadi EK, Hadadian M (2012) Effect of calcination temperature on structural, vibrational, optical, and rheological properties of zirconia nanoparticles. Ceram Int 38:1771–1777. doi:10.1016/j.ceramint.2011.09.063

Goharshadi EK, Samiee S, Hadadian M (2013) Nanofluids for heat transfer enhancement—a review. Phys Chem Res 1:1–33

Gondal MA, Dastageer MA, Khalil A (2009) Synthesis of nano-WO_3 and its catalytic activity for enhanced antimicrobial process for water purification using laser induced photo-catalysis. Catal Commun 11:214–219. doi:10.1016/j.catcom.2009.10.011

Gondal MA, Bagabas A, Dastageer A, Khalil A (2010) Synthesis, characterization, and antimicrobial application of nano-palladium-doped nano-WO_3. J Mol Catal A Chem 323:78–83. doi:10.1016/j.molcata.2010.03.019

Goodenough JB, Hamnett A, Huber G, Hullinger F, Ramasesha SK, Madelung O, Werheit H (1984) Physics of non-tetrahedrally bonded binary compounds III/Physik Der Nicht-Tetraedrisch Gebundenen Binären Verbindungen III. Springer, New York

Haisheng C, Yulong D, Chunqing T (2007) Rheological behaviour of nanofluids. New J Phys 9:367

He Y, Jin Y, Chen H, Ding Y, Cang D, Lu H (2007) Heat transfer and flow behaviour of aqueous suspensions of TiO_2 nanoparticles (nanofluids) flowing upward through a vertical pipe. Int J Heat Mass Transf 50:2272–2281. doi:10.1016/j.ijheatmasstransfer.2006.10.024

Ho CJ, Chen WC (2013) An experimental study on thermal performance of Al_2O_3/water nanofluid in a minichannel heat sink. Appl Therm Eng 50:516–522. doi:10.1016/j.applthermaleng.2012.07.037

Jiang L, Gao L, Sun J (2003) Production of aqueous colloidal dispersions of carbon nanotubes. J Colloid Interface Sci 260:89–94. doi:10.1016/S0021-9797(02)00176-5

Kulkarni DP, Das DK, Chukwu GA (2006) Temperature dependent rheological property of copper oxide nanoparticles suspension (nanofluid). J Nanosci Nanotechnol 6:1150–1154. doi:10.1166/jnn.2006.187

Li Y, Zhou JE, Tung S, Schneider E, Xi S (2009) A review on development of nanofluid preparation and characterization. Powder Technol 196:89–101. doi:10.1016/j.powtec.2009.07.025

Mahbubul IM, Saidur R, Amalina MA (2012) Latest developments on the viscosity of nanofluids. Int J Heat Mass Transf 55:874–885. doi:10.1016/j.ijheatmasstransfer.2011.10.021

Mariano A, Pastoriza-Gallego MJ, Lugo L, Camacho A, Canzonieri S, Piñeiro MM (2013) Thermal conductivity, rheological behaviour and density of non-Newtonian ethylene glycol-based SnO_2 nanofluids. Fluid Phase Equilib 337:119–124. doi:10.1016/j.fluid.2012.09.029

Moosavi M, Goharshadi EK, Youssefi A (2010) Fabrication, characterization, and measurement of some physicochemical properties of ZnO nanofluids. Int J Heat Fluid Flow 31:599–605. doi:10.1016/j.ijheatfluidflow.2010.01.011

Namburu PK, Kulkarni DP, Dandekar A, Das DK (2007a) Experimental investigation of viscosity and specific heat of silicon dioxide nanofluids. Micro Nano Lett 2:67–71

Namburu PK, Kulkarni DP, Misra D, Das DK (2007b) Viscosity of copper oxide nanoparticles dispersed in ethylene glycol and water mixture. Exp Therm Fluid Sci 32:397–402. doi:10.1016/j.expthermflusci.2007.05.001

Nguyen CT, Desgranges F, Galanis N, Roy G, Maré T, Boucher S, Angue Mintsa H (2008) Viscosity data for Al_2O_3–water nanofluid—hysteresis: is heat transfer enhancement using nanofluids reliable? Int J Therm Sci 47:103–111. doi:10.1016/j.ijthermalsci.2007.01.033

Pastoriza-Gallego MJ, Casanova C, Legido JL, Piñeiro MM (2011) CuO in water nanofluid: influence of particle size and polydispersity on volumetric behaviour and viscosity. Fluid Phase Equilib 300:188–196. doi:10.1016/j.fluid.2010.10.015

Patzke GR, Zhou Y, Kontic R, Conrad F (2011) Oxide nanomaterials: synthetic developments, mechanistic studies, and technological innovations. Angew Chem Int Ed 50:826–859

Rao Y (2010) Nanofluids: stability, phase diagram, rheology and applications. Particuology 8:549–555. doi:10.1016/j.partic.2010.08.004

Reid RC, Prausnitz JM, Sherwood TK (1977) The properties of gases and liquids. McGraw-Hill, New York

Servais C, Jones R, Roberts I (2002) The influence of particle size distribution on the processing of food. J Food Eng 51:201–208. doi:10.1016/S0260-8774(01)00056-5

Smith W, Zhang ZY, Zhao YP (2007) Structural and optical characterization of WO_3 nanorods/films prepared by oblique angle deposition. J Vac Sci Technol B. doi:10.1116/1.2799968

Staples CA, Williams JB, Craig GR, Roberts KM (2001) Fate, effects and potential environmental risks of ethylene glycol: a review. Chemosphere 43:377–383. doi:10.1016/S0045-6535(00)00148-X

Svensson JSEM, Granqvist CG (1984) Electrochromic tungsten oxide films for energy efficient windows. Sol Energy Mater 11:29–34. doi:10.1016/0165-1633(84)90025-X

Taherzadeh MJ, Adler L, Lidén G (2002) Strategies for enhancing fermentative production of glycerol—a review. Enzyme Microb Technol 31:53–66. doi:10.1016/S0141-0229(02)00069-8

Tauc J, Grigorovici R, Vancu A (1966) Optical properties and electronic structure of amorphous germanium. Phys Status Solidi (b) 15:627–637. doi:10.1002/pssb.19660150224

Vakili-Nezhaad G, Dorany A (2012) Effect of single-walled carbon nanotube on the viscosity of lubricants. Energy Procedia 14:512–517. doi:10.1016/j.egypro.2011.12.967

Wang J Khoo E, Lee PS, Ma J (2008) Synthesis, assembly, and electrochromic properties of uniform crystalline WO_3 nanorods. J Phys Chem C 112:14306

White F (2005) Viscous fluid flow. McGraw-Hill, New York

Yaws CL (1997) Physical properties—a guide to the physical, thermodynamic and transport property data of industrially important chemical compounds. McGraw Hill, New York

Yeganeh M, Shahtahmasebi N, Kompany A, Goharshadi EK, Youssefi A, Šiller L (2010) Volume fraction and temperature variations of the effective thermal conductivity of nanodiamond fluids in deionized water International. J Heat Mass Transf 53:3186–3192. doi:10.1016/j.ijheatmasstransfer.2010.03.008

Yoffe AD (1993) Low-dimensional systems: quantum size effects and electronic properties of semiconductor microcrystallites (zero-dimensional systems) and some quasi-two-dimensional systems. Adv Phys 42:173–262. doi:10.1080/00018739300101484

Zheng H, Tachibana Y, Kalantar-zadeh K (2010) Dye-sensitized solar cells based on WO_3. Langmuir 26:19148–19152. doi:10.1021/la103692y

Zheng H, Ou JZ, Strano MS, Kaner RB, Mitchell A, Kalantar-zadeh K (2011) nanostructured tungsten oxide—properties. Synth Appl Adv Funct Mater 21:2175–2196